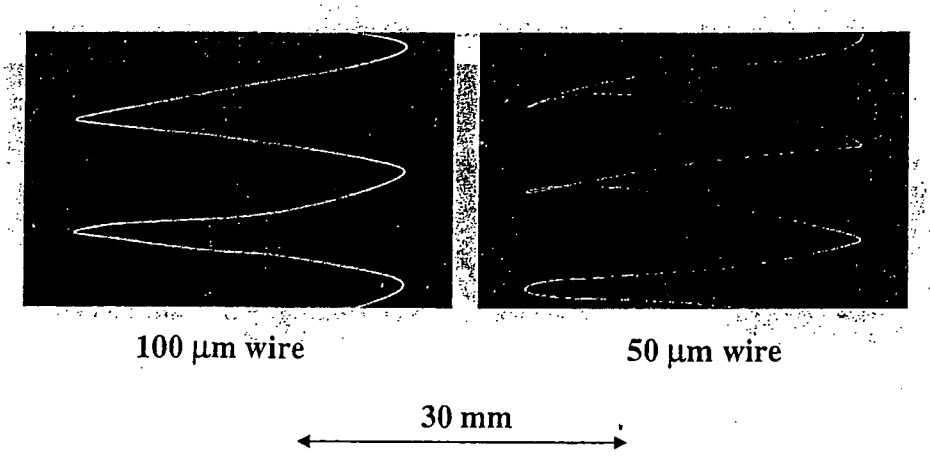

Fig. 5. Radiograms of tungsten wires coiled around PMMA rods.

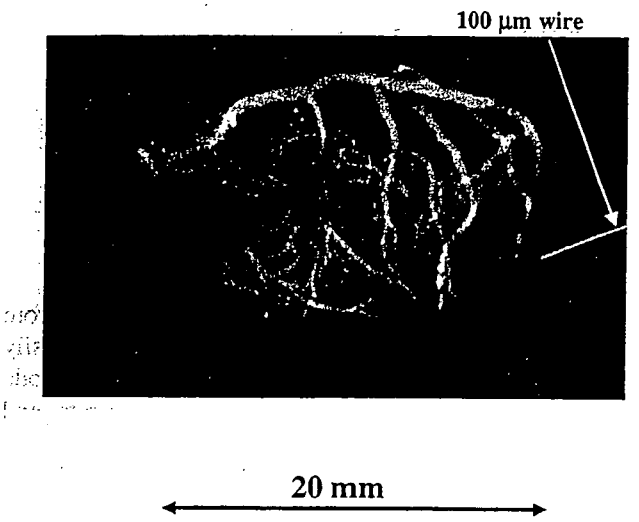

Fig. 6. Angiograms of extracted rabbit heart using iodine microspheres.

image contrast hardly varied with decreases in the wire diameter, a 50-μm-diameter wire could be observed clearly.

Figures 6 and 7 show angiograms of a rabbit heart and a thigh, respectively, with an exposure time of 300 s. The coronary arteries in the heart and fine blood vessels in the thigh with diameters of approximately 100 μm were visible. Figure 8 shows an angiogram of a dog heart in a 100-mm-thick water phantom with an exposure time of 1,500 s. Because the size of the dog heart is almost the same as that of a human heart, human coronary arteries can be observed. For comparison, we show a three-dimensional (3D) image of the coronary arteries constructed from X-ray CT images taken by Pascal (Digital Culture Tech. Corp.) with a tungsten X-ray tube (Fig. 9). This heart was the same as that used in K-edge angiography and was observed from the same direction by rotating the three-dimensional (3D) image; CT angiography was performed without using the water phantom. Using this 3D angiography achieved with a multislice helical CT, fine blood vessels were not observed at all.

5. Discussion

In the present research, we employed an X-ray generator with a cerium-target tube and succeeded in producing cerium characteristic X-rays, which can be absorbed easily by iodine-based contrast media. Both the characteristic and bremsstrahlung X-ray intensities increased with tube voltage

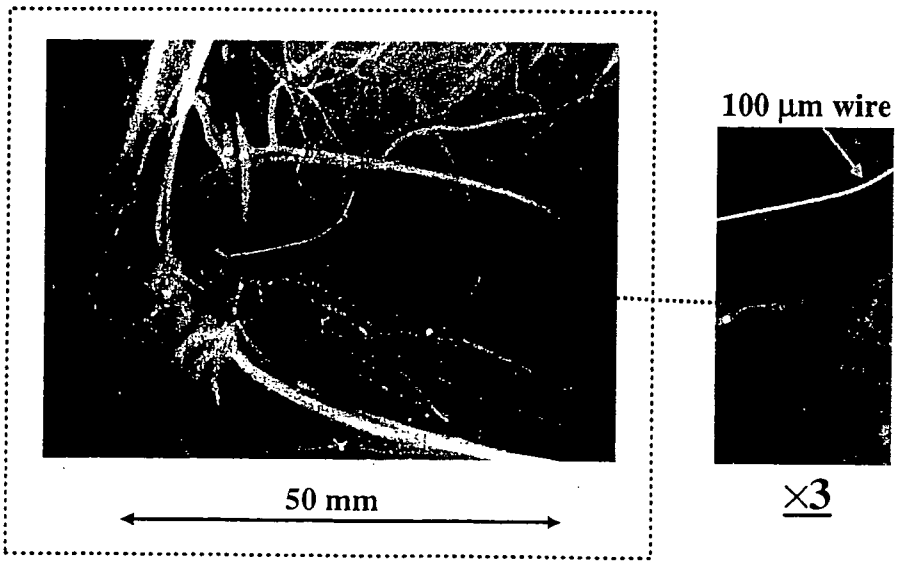

Fig. 7. Angiogram of rabbit thigh using iodine microspheres.

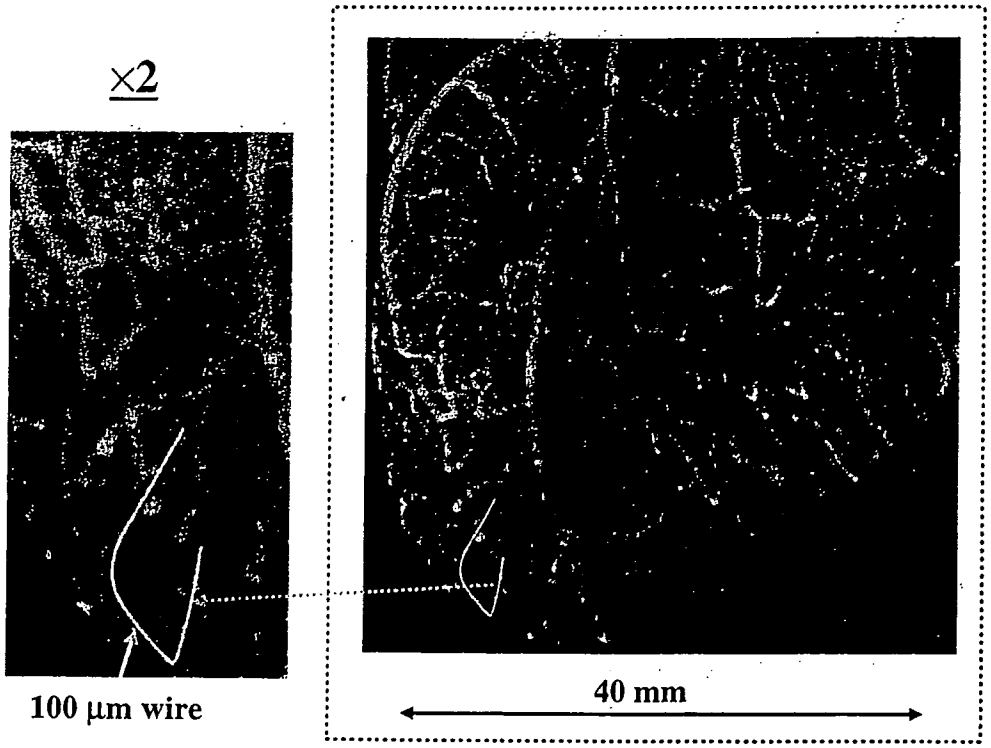

Fig. 8. Angiogram of extracted dog heart in 100-mm-thick water phantom using iodine microspheres.

Fig. 9. Three-dimensional image of coronary arteries constructed from X-ray CT images taken by Pascal.

without filtering. Using the filter to absorb Kβ and bremsstrahlung X-rays, Kα rays were left, and we performed K-edge angiography using the filter with a tube voltage of 60 kV. To produce clean characteristic X-rays without using the filter, the angle dependence of the bremsstrahlung intensity should be considered, since bremsstrahlung rays are not emitted in the direction opposite that of the electron trajectory in Sommerfeld's theory.[18]

Currently, angiography is performed using both the bremsstrahlung and characteristic X-rays produced from a tungsten X-ray tube. However, enhanced K-edge angiography in this work was primarily performed using cerium Kα rays. Using the filter, the maximum number of Kα photons was approximately 3×10^7 photons/(cm^2·s) at 1.0 m from the source, and the photon count rate can be increased easily by improving the target. For example, a new rotation anode tube has been designed to increase the X-ray dose rate, and the rate can be increased by increasing the anode diameter.

In energy-selective imaging including K-edge angiography, the filtering effect of the absorber should be considered, and the X-ray spectra using the filter at a tube voltage of 60 kV hardly varies with changes in the thickness of the water phantom according to the spectrum estimation. Due to the absorption coefficient, Kβ rays are also useful for angiography, and both the Kα and Kβ rays can be left using a cerium oxide filter with a surface density of approximately 10 mg/cm^2. In addition, an aluminum filter with a thickness of approximately 3.0 mm is useful in absorbing unnecessary bremsstrahlung X-rays with energies lower than the K-absorption edge.

Acknowledgment

This work was supported by Grants-in-Aid for Scientific Research (13470154, 13877114, 16591181, and 16591222) and Advanced Medical Scientific Research from MECSST, Health and Labor Sciences Research Grants (RAMT-nano-001, RHGTEFB-genome-005 and RHGTEFB-saisei-003), Grants from the Keiryo Research Foundation, The Promotion and Mutual Aid Corporation for Private Schools of Japan, Japan Science and Technology Agency (JST), and the New Energy and Industrial Technology Development Organization (NEDO, Industrial Technology Research Grant Program in '03).

1) A. Akisada, M. Ando, K. Hyodo, S. Hasegawa, K. Konishi, K. Nishimura, A. Maruhashi, F. Toyofuku, A. Suwa and K. Kohra: Nucl. Instrum. Methods Phys. Res., Sect. A **246** (1986) 713.
2) A. C. Thompson, H. D. Zeman, G. S. Brown, J. Morrison, P. Reiser,

V. Padmanabahn, L. Ong, S. Green, J. Giacomini, H. Gordon and E. Rubenstein: Rev. Sci. Instrum. **63** (1992) 625.
3) H. Mori *et al.*: Radiology **201** (1996) 173.
4) K. Hyodo, M. Ando, Y. Oku, S. Yamamoto, T. Takeda, Y. Itai, S. Ohtsuka, Y. Sugishita and J. Tada: J. Synchrotron Radiat. **5** (1998) 1123.
5) T. J. Davis, D. Gao, T. E. Gureyev, A. W. Stevenson and S. W. Wilkins: Nature **373** (1995) 595.
6) A. Momose, T. Takeda, Y. Itai and K. Hirano: Nat. Med. **2** (1996) 473.
7) M. Ando, A. Maksimenko, H. Sugiyama, W. Pattanasiriwisawa, K. Hyodo and C. Uyama: Jpn. J. Appl. Phys. **41** (2002) L1016.
8) E. Sato, S. Kimura, S. Kawasaki, H. Isobe, K. Takahashi, Y. Tamakawa and T. Yanagisawa: Rev. Sci. Instrum. **61** (1990) 2343.
9) A. Shikoda, E. Sato, M. Sagae, T. Oizumi, Y. Tamakawa and T. Yanagisawa: Rev. Sci. Instrum. **65** (1994) 850.
10) K. Takahashi, E. Sato, M. Sagae, T. Oizumi, Y. Tamakawa and T. Yanagisawa: Jpn. J. Appl. Phys. **33** (1994) 4146.
11) E. Sato, K. Takahashi, M. Sagae, S. Kimura, T. Oizumi, Y. Hayasi, Y. Tamakawa and T. Yanagisawa: Med. Biol. Eng. Comput. 32 (1994) 289.
12) E. Sato, Y. Hayasi, R. Germer, E. Tanaka, H. Mori, T. Kawai, T. Ichimaru, K. Takayama and H. Ido: Rev. Sci. Instrum. **74** (2003) 5236.
13) E. Sato, Y. Hayasi, R. Germer, E. Tanaka, H. Mori, T. Kawai, T. Ichimaru, S. Sato, K. Takayama and H. Ido: J. Electron Spectrosc. Relat. Phenom. C **137–140** (2004) 713.
14) E. Sato, Y. Hayasi, R. Germer, E. Tanaka, H. Mori, T. Kawai, H. Obara, T. Ichimaru, K. Takayama and H. Ido: Jpn. J. Med. Phys. **20** (2003) 123.
15) E. Sato, E. Tanaka, H. Mori, T. Kawai, T. Ichimaru, S. Sato, K. Takayama and H. Ido: Med. Phys. **32** (2005) 49.
16) E. Sato, E. Tanaka, H. Mori, T. Kawai, T. Ichimaru, S. Sato, K. Takayama and H. Ido: Med. Phys. **31** (2004) 3017.
17) E. Sato, K. Sato and Y. Tamakawa: Annu. Rep. Iwate Med. Univ. School Lib. Arts Sci. **35** (2000) 13.
18) B. K. Agarwal: *X-ray Spectroscopy* (Springer-Verlag, New York, 1991) 2nd ed., p. 18.

Japanese Journal of Applied Physics
Vol. 44, No. 12, 2005, pp. 8716–8721

Enhanced K-edge Angiography Utilizing Tantalum Plasma X-ray Generator in Conjunction with Gadolinium-Based Contrast Media

Eiichi SATO, Yasuomi HAYASI, Koji KIMURA[1], Etsuro TANAKA[2], Hidezo MORI[3], Toshiaki KAWAI[4], Takashi INOUE[5], Akira OGAWA[5], Shigehiro SATO[6], Kazuyoshi TAKAYAMA[7], Jun ONAGAWA[8] and Hideaki IDO[8]

Department of Physics, Iwate Medical University, 3-16-1 Honchodori, Morioka 020-0015, Japan
[1]*Department of Physiology, Tokai University School of Medicine, Boseidai, Isehara, Kanagawa 259-1193, Japan*
[2]*Department of Nutritional Science, Faculty of Applied Bio-science, Tokyo University of Agriculture, 1-1-1 Sakuragaoka, Setagaya-ku, Tokyo 156-8502, Japan*
[3]*Department of Cardiac Physiology, National Cardiovascular Center Research Institute, 5-7-1 Fujishirodai, Suita, Osaka 565-8565, Japan*
[4]*Electron Tube Division #2, Hamamatsu Photonics K.K., 314-5 Shimokanzo, Toyooka Village, Iwata, Shizuoka 438-0193, Japan*
[5]*Department of Neurosurgery, School of Medicine, Iwate Medical University, 19-1 Uchimaru, Morioka 020-8505, Japan*
[6]*Department of Microbiology, School of Medicine, Iwate Medical University, 19-1 Uchimaru, Morioka 020-8505, Japan*
[7]*Shock Wave Research Center, Institute of Fluid Science, Tohoku University, 2-1-1 Katahira, Sendai 980-8577, Japan*
[8]*Department of Applied Physics and Informatics, Faculty of Engineering, Tohoku Gakuin University, 1-13-1 Chuo, Tagajo, Miyagi 985-8537, Japan*

(Received June 5, 2005; accepted August 17, 2005; published December 8, 2005)

The tantalum plasma flash X-ray generator is useful for performing high-speed enhanced K-edge angiography using cone beams because K-series characteristic X-rays from the tantalum target are absorbed effectively by gadolinium-based contrast media. In the flash X-ray generator, a 150 nF condenser is charged up to 80 kV by a power supply, and flash X-rays are produced by the discharging. The X-ray tube is a demountable cold-cathode diode, and the turbomolecular pump evacuates air from the tube with a pressure of approximately 1 mPa. Since the electric circuit of the high-voltage pulse generator employs a cable transmission line, the high-voltage pulse generator produces twice the potential of the condenser charging voltage. At a charging voltage of 80 kV, the estimated maximum tube voltage and current were approximately 160 kV and 40 kA, respectively. When the charging voltage was increased, the K-series characteristic X-ray intensities of cerium increased. The K lines were clean and intense, and hardly any bremsstrahlung rays were detected. The X-ray pulse widths were approximately 100 ns, and the time-integrated X-ray intensity had a value of approximately 300 μGy at 1.0 m from the X-ray source with a charging voltage of 80 kV. Angiography was performed using a filmless computed radiography (CR) system and gadolinium-based contrast media. In the angiography of nonliving animals, we observed fine blood vessels of approximately 100 μm with high contrasts. [DOI: 10.1143/JJAP.44.8716]

KEYWORDS: angiography, gadolinium-based contrast media, characteristic X-rays, quasi-monochromatic X-rays, tantalum K lines

1. Introduction

Enhanced K-edge angiography[1–4] has been performed utilizing monochromatic parallel X-ray beams produced from synchrotron orbital radiation using a monochrocollimator. The photon energies of the beams are approximately 35 keV, and are absorbed effectively by iodine-based contrast media with a K-absorption edge of 33.2 keV. Nowadays, an X-ray generator with a cerium-target tube[5] can be used in order to perform the K-edge angiography because K-series characteristic X-rays with photon energies just beyond the K-edge are absorbed effectively by iodine.

To perform high-speed biomedical radiography, we have developed several different high-dose-rate X-ray generators corresponding to specific objectives. For example, flash X-ray generators[6–9] with cold-cathode tubes produce extremely short X-ray pulses with durations of less than 1 μs, and the X-ray duration can be controlled accurately from 10 μs to 1.0 ms in cases where stroboscopic X-ray generators[10,11] utilizing hot-cathode triodes are employed.

Recently, although clean K-series characteristic X-rays of copper[12] and nickel[13] have been produced using plasma flash X-ray generators, low-intensity bremsstrahlung X-rays have been observed using a molybdenum target.[14] Therefore, we have performed preliminary experiments for producing clean high-photon-energy characteristic X-rays from molybdenum, silver and cerium targets using a compact flash X-ray generator with a disk-cathode tube,[15] and have succeeded in producing clean characteristic X-rays using the angle dependence of bremsstrahlung X-ray distributions. However, the X-ray intensity should be increased to a sufficient level for iodine angiography by increasing the electrostatic energies in the generator.

Since K-series characteristic X-rays from ytterbium, tantalum, and tungsten targets are absorbed effectively by gadolinium-based contrast media used in MRA, these X-rays are very useful for performing enhanced K-edge angiography. As compared with K-edge angiography using an iodine medium with an X-ray photon energy of 35 keV, the absorbed dose can be decreased easily in cases where the gadolinium medium is employed.

In the present research, we developed an intense quasi-monochromatic plasma flash X-ray generator with a tantalum target tube, and used it to perform a preliminary study on angiography achieved with tantalum K-series characteristic X-rays.

2. Principle of Angiography

Figure 1 shows the mass attenuation coefficients of gadolinium at the selected energies; the coefficient curve is discontinuous at the gadolinium K-edge. The average photon energy of the tantalum Kα lines is shown above the gadolinium K-edge. The average photon energy of tantalum Kα lines is 57.1 keV, and gadolinium contrast media with a K-absorption edge of 50.2 keV absorb the lines easily. Therefore, blood vessels were observed with high contrasts.

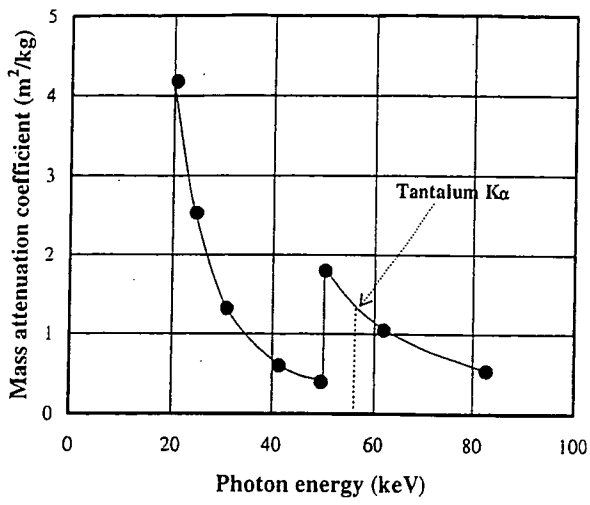

Fig. 1. Mass attenuation coefficient of gadolinium. The average photon energy of tantalum Kα lines is shown above the gadolinium K-edge.

3. Generator

3.1 *High-voltage circuit*

Figure 2 shows a block diagram including the electric circuit of a high-intensity plasma flash X-ray generator. The generator consists of the following essential components: a high-voltage power supply, a high-voltage condenser with a capacity of approximately 150 nF, an air gap switch, a turbomolecular pump, a thyratron pulse generator as a trigger device, and a flash X-ray tube. In this generator, a coaxial cable transmission line is employed in order to increase maximum tube voltage using high-voltage reflection. The high-voltage main condenser is charged up to 80 kV by the power supply, and electric charges in the condenser are discharged to the tube through the four cables after closing the gap switch with the trigger device.

3.2 *X-ray tube*

The X-ray tube is a demountable cold-cathode diode that is connected to the turbomolecular pump with a pressure of approximately 1 mPa (Fig. 3). This tube consists of the following major parts: a ring-shaped graphite cathode with an inside diameter of 4.5 mm, a stainless-steel vacuum chamber, a nylon insulator, a polyethylene terephthalate (Mylar) X-ray window 0.25 mm in thickness, and a rod-shaped tantalum target 3.0 mm in diameter. The distance between the target and cathode electrodes can be regulated from the outside of the tube, and is set to 1.5 mm. As electron beams from the cathode electrode are roughly converged to the target by the electric field in the tube, evaporation leads to the formation of weakly ionized plasma, consisting of tantalum ions and electrons, around the target. Because bremsstrahlung rays are not emitted in the opposite direction to that of the electron trajectory in Sommerfeld's theory[16] (Fig. 4), tantalum K-series characteristic X-rays can be produced without using a filter.

4. Characteristics

4.1 *Tube voltage and current*

In this generator, it was difficult to measure the tube voltage and current since the tube voltages were high, and there was no space to set a current transformer for measuring the tube current. Currently, the voltage and current roughly display damped oscillations. When the charging voltage was increased, both the maximum tube voltage and current increased. At a charging voltage of 80 kV, the estimated maximum values of the tube voltage and current were approximately 160 kV (two times the charging voltage) and 40 kA, respectively.

4.2 *X-ray output*

The X-ray output pulse was detected using a combination of a plastic scintillator and a photomultiplier (Fig. 5). The X-ray pulse height substantially increased with charging

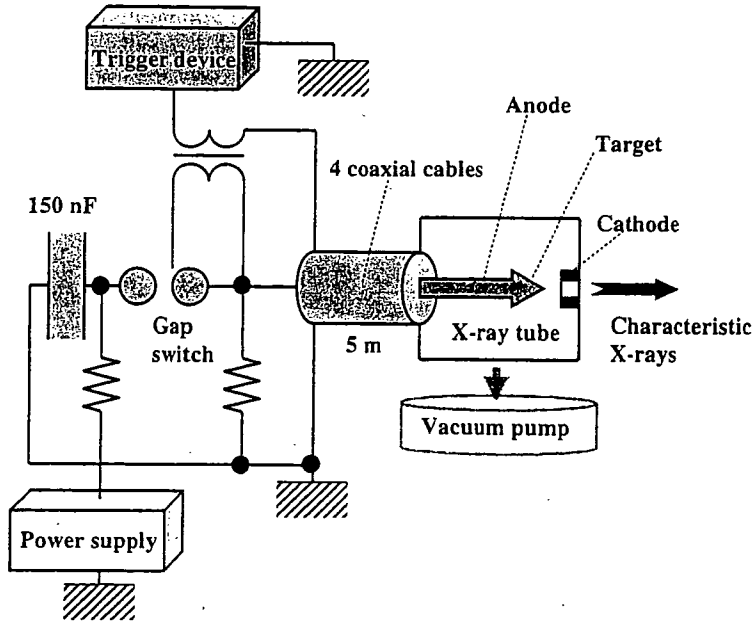

Fig. 2. Block diagram including high-voltage circuit of intense quasi-monochromatic plasma flash X-ray generator with tantalum-target tube.

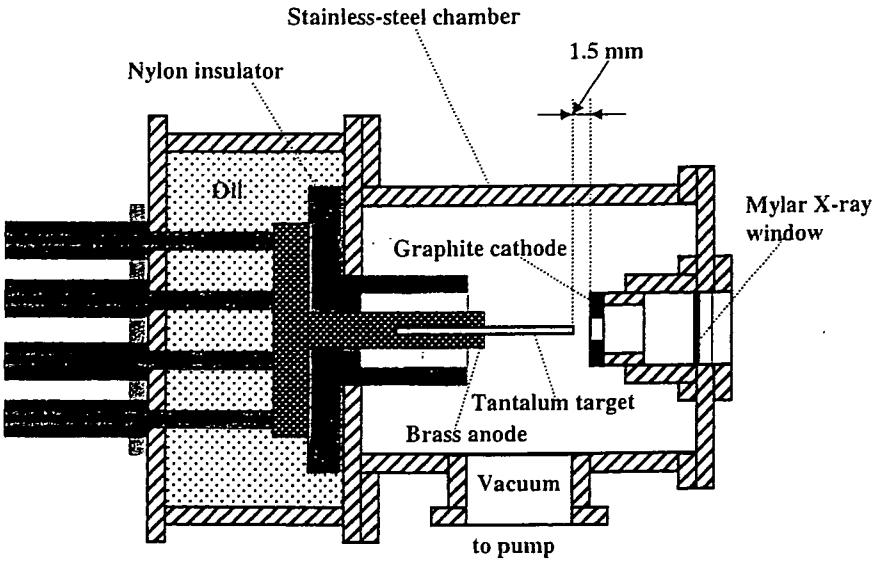

Fig. 3. Schematic drawing of flash X-ray tube with rod-shaped tantalum target.

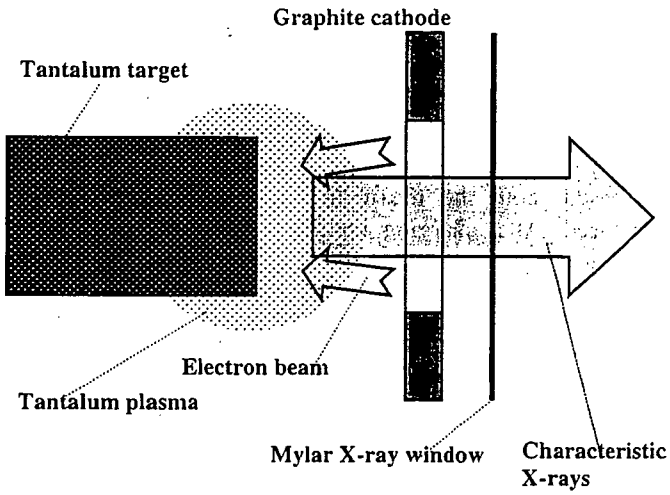

Fig. 4. Irradiation of K-series characteristic X-rays of tantalum.

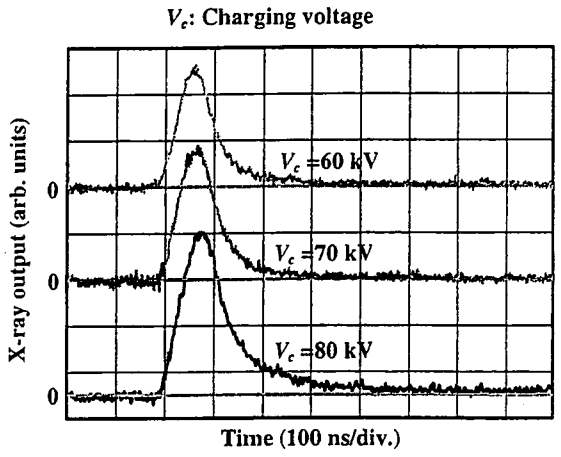

Fig. 5. X-ray outputs detected using combination of plastic scintillator and photomultiplier.

voltage. The X-ray pulse widths were approximately 100 ns, and the time-integrated X-ray intensity measured by a thermoluminescence dosimeter (Kyokko TLD Reader 1500 having MSO-S elements without energy compensation) had a value of approximately 300 μGy per pulse at 1.0 m from the X-ray source with a charging voltage of 80 kV.

4.3 X-ray source

In order to observe the characteristic X-ray source, we employed a 100-μm-diameter pinhole camera and an X-ray film (Polaroid XR-7) (Fig. 6). When the charging voltage was increased, the plasma X-ray source grew, and both spot dimension and intensity increased. Because the X-ray intensity is the highest at the center of the spot, both the dimension and intensity decreased as the thickness of a filter for absorbing X-rays increased and as the pinhole diameter decreased.

4.4 X-ray spectra

X-ray spectra were measured using a transmission-type spectrometer[14] with a lithium fluoride curved crystal 0.5 mm

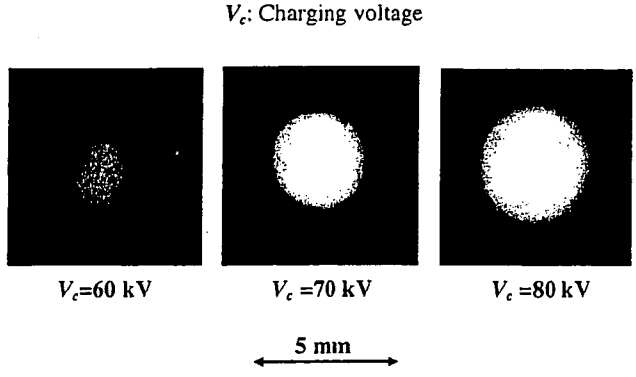

Fig. 6. Images of characteristic X-ray source obtained using pinhole camera with changes in charging voltage.

in thickness. The X-ray intensities of the spectra were detected by an imaging plate of a CR system[17] (Konica Regius 150) with a wide dynamic range, and relative X-ray intensity was calculated from Dicom original digital data corresponding to X-ray intensity; the data was scanned by a

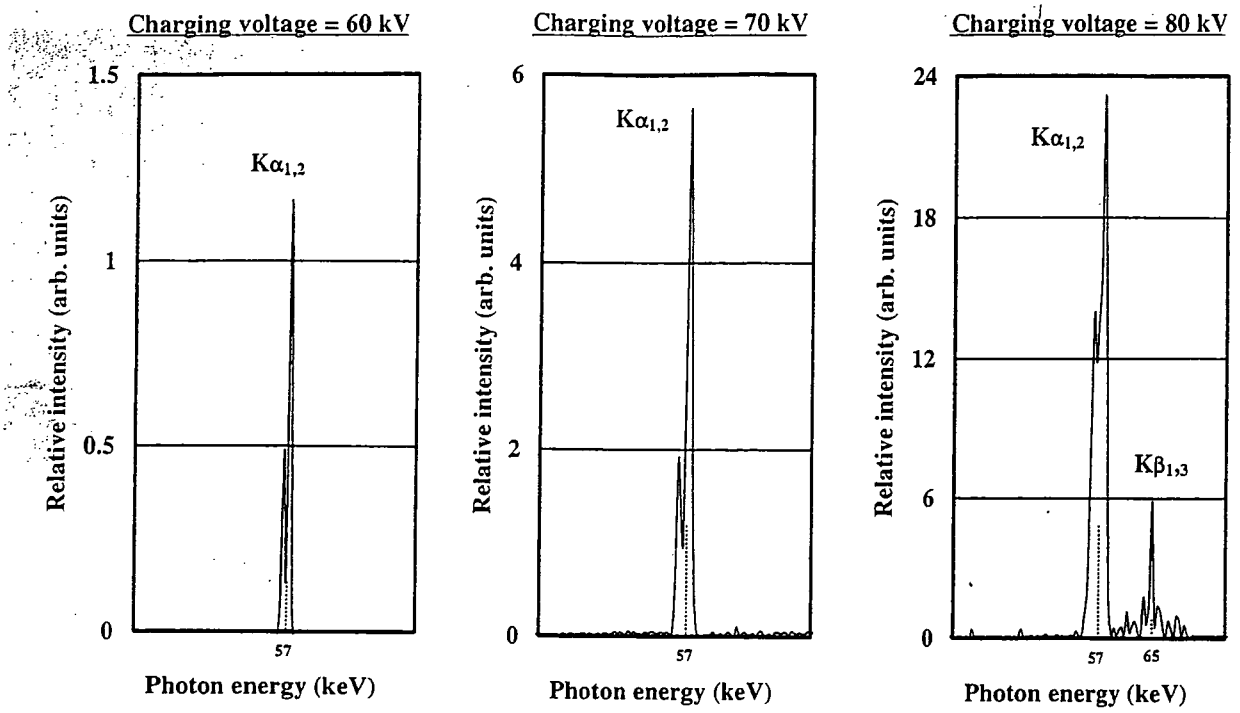

Fig. 7. X-ray spectra from tantalum target. Spectra were measured using a transmission-type spectrometer with a lithium fluoride curved crystal.

Dicom viewer in the filmless CR system. Subsequently, the relative X-ray intensity as a function of the data was calibrated using a conventional X-ray generator, and we confirmed that the intensity was proportional to the exposure time. Figure 7 shows measured spectra from the tantalum target. We observed clean K-series lines, while bremsstrahlung rays were hardly detected. The characteristic X-ray intensity substantially increased with charging voltage.

5. Angiography

Flash angiography was performed using the CR system at 1.2 m from the X-ray source, and the charging voltage was 80 kV. First, rough measurements of spatial resolution were made using wires. Figure 8 shows radiograms of tungsten wires in a rod made of poly(methyl methacrylate) (PMMA). Although the image contrast decreased slightly with wire diameter, due to blurring of the image caused by the sampling pitch of 87.5 μm, a 50-μm-diameter wire could be observed. Because the tungsten wires transmitted the characteristic X-rays easily, low-contrast radiograms were obtained.

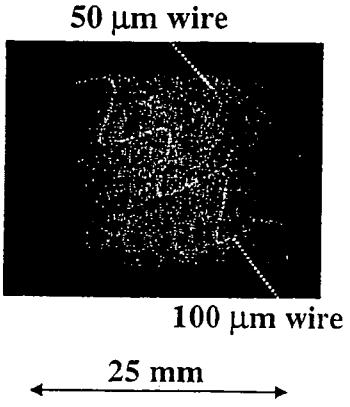

Fig. 8. Radiograms of tungsten wires in PMMA rod.

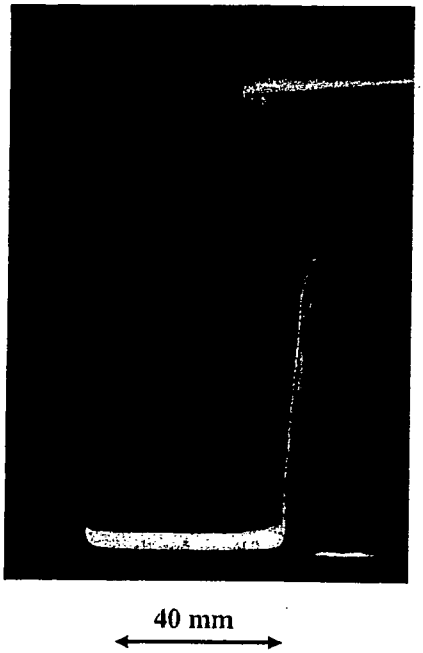

Fig. 9. Radiogram of water (20% gadolinium oxide suspension) falling into polypropylene beaker from glass test tube.

The image of water (gadolinium oxide suspension of 20%) falling into a polypropylene beaker from a plastic test tube is shown in Fig. 9. The diameter of gadolinium oxide powder ranges from 1 to 10 μm. Because the X-ray duration was about 100 ns, the stop-motion image of water could be obtained.

Figure 10 shows an angiogram of poly(tetrafluoroethylene) (Teflon) tubes of 0.5 and 1.0 mm bore diameter in a

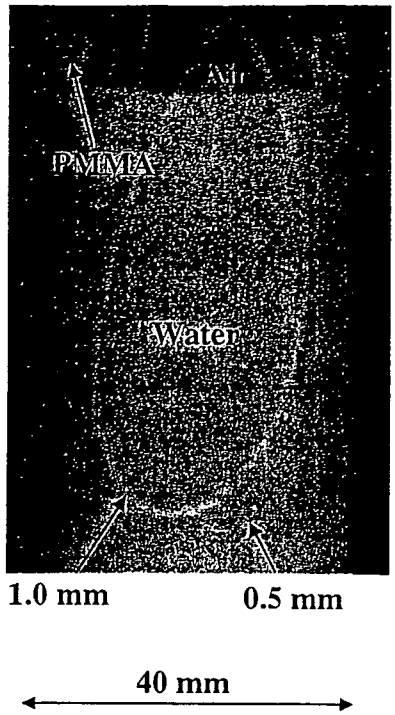

Fig. 10. Angiography of Teflon tube using contrast medium which contains approximately 65% gadodiamidehydrate.

PMMA case using a contrast medium which contains approximately 65% gadodiamidehydrate; the 0.5 mm tube can be observed easily. Figure 11 shows an angiogram of a rabbit head using gadolinium oxide powder, and fine blood vessels of approximately 100 μm were visible.

6. Discussion

In summary, we succeeded in producing K-series characteristic X-rays of tantalum and in performing K-edge angiography using gadolinium contrast media with a K-edge of 50.2 keV; this K-edge angiography could be a useful technique for reducing the dose absorbed by patients. Although we employed tantalum Kα (57.1 keV) and Kβ (approximately 65 keV) rays, Kβ rays should be absorbed using an ytterbium oxide filter in order to increase the image contrast of blood vessels. In addition, L-series characteristic rays should be absorbed before angiography using a tungsten or an ytterbium oxide filter. In these cases, the photon energies of the K-absorption edges of tungsten and ytterbium are 69.5 and 61.3 keV, respectively.

In cases where a high tube voltage beyond the critical excitation potential is applied, the optimum intensity for angiography can be controlled because the K-series characteristic intensity substantially increases with charging voltage. In this research, the generator-produced instantaneous number of K photons was approximately 1×10^9 photons/cm^2 per pulse at 1.0 m from the source.

Using this flash X-ray generator, because the photon energy of characteristic X-rays can be selected, quasi-monochromatic imaging, such as enhanced K-edge angiography using iodine contrast media and mammography, can be performed. In addition, steady-state monochromatic X-rays can be produced by a similar tube utilizing a hot cathode and a constant high-voltage power supply. In conjunction with the fine focusing technique, these monochromatic X-ray generators could be employed to perform K-edge angiography and X-ray phase-contrast radiography for edge enhancement.

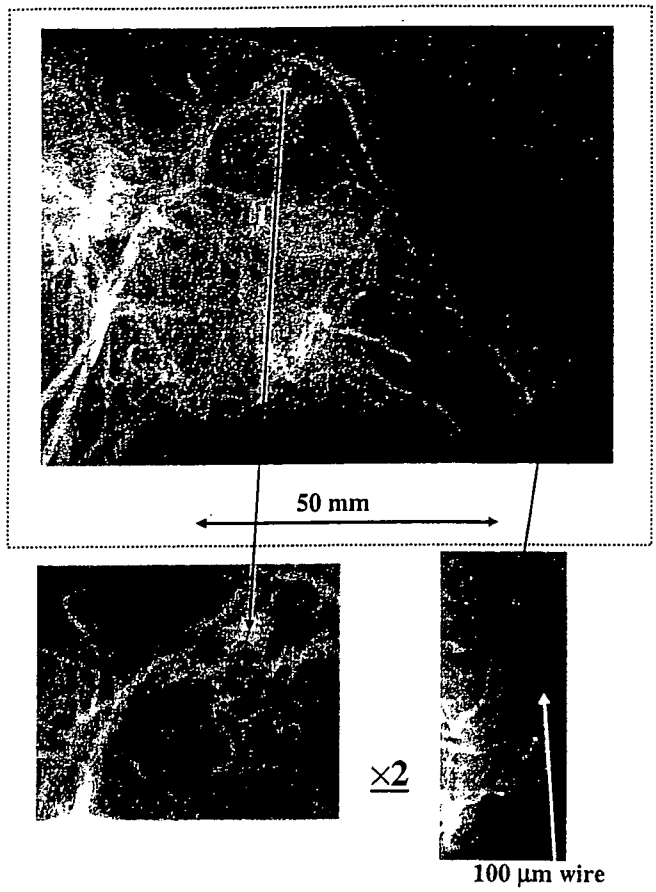

Fig. 11. Angiography of rabbit head using gadolinium oxide powder.

Acknowledgment

This work was supported by Grants-in-Aid for Scientific Research (13470154, 13877114, 16591181, and 16591222) and Advanced Medical Scientific Research from MECSST, Health and Labor Sciences Research Grants (RAMT-nano-001, RHGTEFB-genome-005 and RHGTEFB-saisei-003), Grants from the Keiryo Research Foundation, The Promotion and Mutual Aid Corporation for Private Schools of Japan, the Japan Science and Technology Agency (JST), and the New Energy and Industrial Technology Development Organization (NEDO, Industrial Technology Research Grant Program in '03).

1) A. Akisada, M. Ando, K. Hyodo, S. Hasegawa, K. Konishi, K. Nishimura, A. Maruhashi, F. Toyofuku, A. Suwa and K. Kohra: Nucl. Instrum. Methods Phys. Res., Sect. A **246** (1986) 713.
2) A. C. Thompson, H. D. Zeman, G. S. Brown, J. Morrison, P. Reiser, V. Padmanabahn, L. Ong, S. Green, J. Giacomini, H. Gordon and E. Rubenstein: Rev. Sci. Instrum. **63** (1992) 625.
3) H. Mori *et al.*: Radiology **201** (1996) 173.
4) K. Hyodo, M. Ando, Y. Oku, S. Yamamoto, T. Takeda, Y. Itai, S. Ohtsuka, Y. Sugishita and J. Tada: J. Synchrotron Radiat. 5 (1998) 1123.
5) E. Sato, E. Tanaka, H. Mori, T. Kawai, T. Ichimaru, S. Sato, K. Takayama and H. Ido: Med. Phys. **31** (2004) 3017.
6) E. Sato, S. Kimura, S. Kawasaki, H. Isobe, K. Takahashi, Y. Tamakawa and T. Yanagisawa: Rev. Sci. Instrum. **61** (1990) 2343.
7) A. Shikoda, E. Sato, M. Sagae, T. Oizumi, Y. Tamakawa and T.

Yanagisawa: Rev. Sci. Instrum. **65** (1994) 850.
8) K. Takahashi, E. Sato, M. Sagae, T. Oizumi, Y. Tamakawa and T. Yanagisawa: Jpn. J. Appl. Phys. **33** (1994) 4146.
9) E. Sato, K. Takahashi, M. Sagae, S. Kimura, T. Oizumi, Y. Hayasi, Y. Tamakawa and T. Yanagisawa: Med. Biol. Eng. Comput. **32** (1994) 289.
10) E. Sato, M. Sagae, K. Takahashi, A. Shikoda, T. Oizumi, Y. Hayasi, Y. Tamakawa and T. Yanagisawa: Med. Biol. Eng. Comput. **32** (1994) 295.
11) E. Sato, Y. Hayasi and Y. Tamakawa: Annu. Rep. Iwate Med. Univ. Lib. Arts Sci. **35** (2000) 1.
12) E. Sato, Y. Hayasi, R. Germer, E. Tanaka, H. Mori, T. Kwai, T. Ichimaru, K. Takayama and H. Ido: Rev. Sci. Instrum. **74** (2003) 5236.
13) E. Sato, Y. Hayasi, R. Germer, E. Tanaka, H. Mori, T. Kawai, T. Ichimaru, S. Sato, K. Takayama and H. Ido: J. Electron Spectrosc. Relat. Phenom. C **137–140** (2004) 713.
14) E. Sato, Y. Hayasi, R. Germer, E. Tanaka, H. Mori, T. Kawai, H. Obara, T. Ichimaru, K. Takayama and H. Ido: Jpn. J. Med. Phys. **20** (2003) 123.
15) E. Sato, E. Tanaka, H. Mori, T. Kawai, T. Ichimaru, S. Sato, K. Takayama and H. Ido: Med. Phys. **32** (2005) 49.
16) B. K. Agarwal: *X-ray Spectroscopy* (Springer-Verlag, New York, 1991) 2nd ed., p. 18.
17) E. Sato, K. Sato and Y. Tamakawa: Annu. Rep. Iwate Med. Univ. Sch. Lib. Arts Sci. **35** (2000) 13.

Compact monochromatic flash x-ray generator utilizing a disk-cathode molybdenum tube

Eiichi Sato[a)]
Department of Physics, Iwate Medical University, 3-16-1 Honchodori Morioka 020-0015, Japan

Etsuro Tanaka
Department of Nutritional Science, Faculty of Applied Bio-science, Tokyo University of Agriculture, Setagayaku 156-8502, Japan

Hidezo Mori
Department of Cardiac Physiology, National Cardiovascular Center Research Institute, Osaka 565-8565 Japan

Toshiaki Kawai
Electron Tube Division #2, Hamamatsu Photonics K. K., Iwata-gun 438-0193, Japan

Toshio Ichimaru
Department of Radiological Technology, School of Health Sciences, Hirosaki University, Hirosaki 036-8564, Japan

Shigehiro Sato
Department of Microbiology, School of Medicine, Iwate Medical University, Morioka 020-8505; Japan

Kazuyoshi Takayama
Shock Wave Research Center, Institute of Fluid Science, Tohoku University, Sendai 980-8577, Japan

Hideaki Ido
Department of Applied Physics and Informatics, Faculty of Engineering, Tohoku Gakuin University, Tagajo 985-8537, Japan

(Received 8 April 2004; revised 16 October 2004; accepted for publication 18 October 2004; published 15 December 2004)

The high-voltage condensers in a polarity-inversion two-stage Marx surge generator are charged from −50 to −70 kV by a power supply, and the electric charges in the condensers are discharged to an x-ray tube after closing gap switches in the surge generator with a trigger device. The x-ray tube is a demountable diode, and the turbo molecular pump evacuates air from the tube with a pressure of approximately 1 mPa. Clean molybdenum Kα lines are produced using a 20 μm-thick zirconium filter, since the tube utilizes a disk cathode and a rod target, and bremsstrahlung rays are not emitted in the opposite direction to that of electron acceleration. At a charging voltage of −70 kV, the instantaneous tube voltage and current were 120 kV and 1.0 kA, respectively. The x-ray pulse widths were approximately 70 ns, and the generator produced instantaneous number of Kα photons was approximately 3×10^7 photons/cm^2 per pulse at 0.5 m from the source of 3.0 mm in diameter. © *2005 American Association of Physicists in Medicine.* [DOI: 10.1118/1.1829247]

Key words: x-ray source, x-ray tube, x-ray spectra, rapid imaging, x-ray beam filtration, monochromatic x ray

I. INTRODUCTION

In recent years, many valuable discoveries have been made in laser technology, and soft x-ray lasers of neonlike argon (46.9 nm, 26.4 eV) have been produced using a gas-discharge capillary.[1–3] In these experiments, the laser energy increased with increases in the capillary length, and these kinds of first discharges can generate hot and dense plasma columns with aspect ratios of 1000:1. However, it is difficult to increase the laser photon energy to 10 keV or beyond.

We have developed several different soft flash x-ray generators[4–8] corresponding to specific radiographic objectives, and a major goal in our research is the development of an intense and clean monochromatic x-ray generator that can impact applications with medical radiography. In view of this situation, we confirmed irradiation of intense K-series characteristic x rays from the plasma axial direction by forming weakly ionized linear plasma.[9–12] In the plasma, bremsstrahlung spectra with photon energies of higher than the K-absorption edge are effectively absorbed and are converted into fluorescent x rays, and the plasma then transmits the fluorescent rays easily. However, the bremsstrahlung x rays are produced using a molybdenum target,[11] since high photon energy bremsstrahlung x rays are not absorbed effectively in the linear plasma.

Without forming the linear plasma, because bremsstrahlung rays are not emitted in the opposite direction to that of electron acceleration, characteristic x rays can be produced by considering the angle dependence of bremsstrahlung x rays. As compared with the plasma generator, the photon

 0094-2405/2005/32(1)/49/6/$22.50

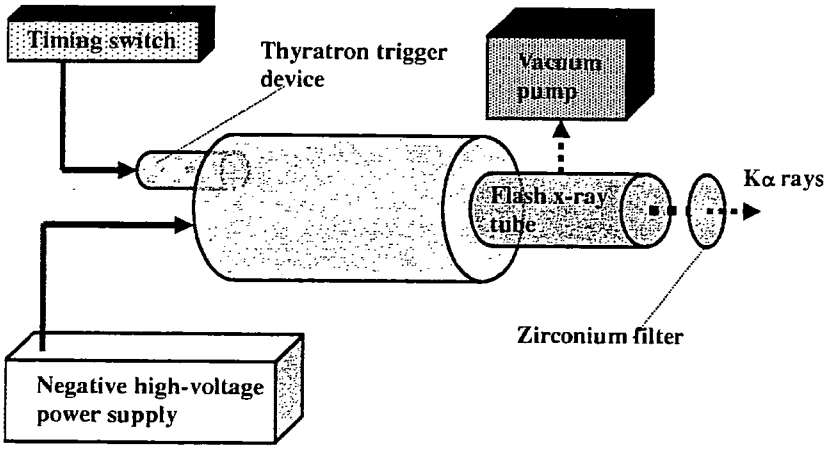

FIG. 1. Block diagram of the compact quasimonochromatic flash x-ray generator with a cold-cathode monochromatic diode.

energy of the characteristic x rays can be increased by increasing the maximum output voltage of the pulse generator, since a multistage Marx generator[13,14] can be employed. In this case, the output voltage is equal to the value of the condenser charging voltage multiplied by the stage number.

In this article, we describe a compact flash x-ray generator utilizing a molybdenum-target radiation tube, used to perform a preliminary experiment for producing clean monochromatic x rays.

II. GENERATOR

A. High-voltage circuit

Figure 1 shows a block diagram of a compact monochromatic flash x-ray generator. This generator consists of the following components: a constant high-voltage power supply, a surge Marx generator with a capacity during main discharge of 425 pF, a thyratron trigger device of the surge generator, a turbo molecular pump, and a flash x-ray tube. Since the electric circuit of the high-voltage pulse generator employs a polarity-inversion two-stage Marx line[13,14] (Fig. 2), the surge generator produces twice the potential of the condenser charging voltage. When two condensers inside of the surge generator are charged from −50 to −70 kV, the ideal output voltage ranges from 100 to 140 kV.

B. X-ray tube

The x-ray tube is a demountable diode type, as illustrated in Fig. 3. This tube is connected to the turbo molecular pump with a pressure of about 1 mPa and consists of the following major devices: a rod-shaped molybdenum target 3.0 mm in diameter, a disk cathode made of graphite, a polyethylene terephthalate (Mylar) x-ray window 0.25 mm in thickness, and a polymethyl methacrylate tube body. The target-cathode space was regulated to 1.0 mm from the outside of the x-ray tube by rotating the anode rod, and the transmission x rays are obtained through a 1.0 mm-thick graphite cathode and an x-ray window. Because bremsstrahlung rays are not emitted in the opposite direction to that of electron acceleration (Fig. 4), molybdenum Kα rays can be produced using a 20 μm-thick zirconium K-edge filter.

III. CHARACTERISTICS

A. Tube voltage and current

Tube voltage and current were measured by a high-voltage divider with an input impedance of 10 kΩ and a current transformer, respectively (Fig. 5). The voltage and current displayed roughly damped oscillations because the discharge resistance in the tube varied rapidly from infinity

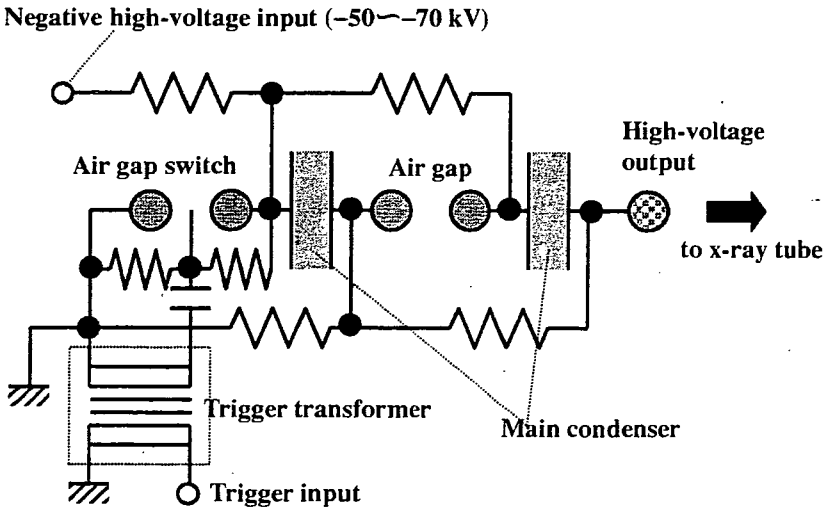

FIG. 2. Circuit diagram of the two-stage surge Marx generator. The generator produces twice the potential of the condenser charging voltage.

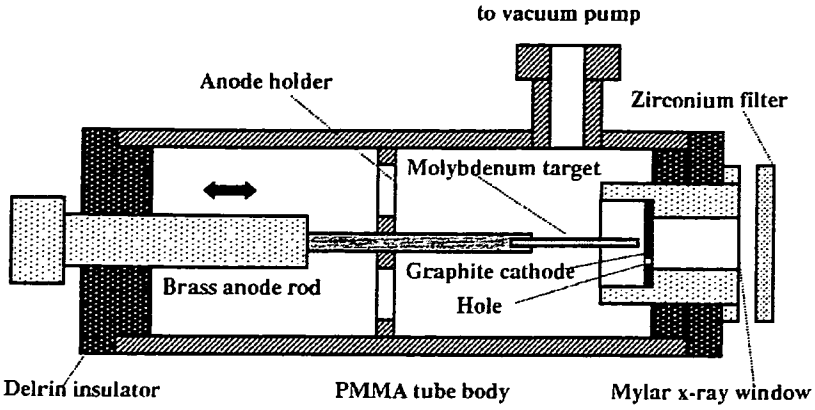

FIG. 3. Schematic drawing of the flash x-ray tube with a rod-shaped molybdenum target and a disk graphite cathode.

to approximately 0 Ω during the discharge. Thus, at the first quarter cycle of the oscillations, when the voltage decreased, the current increased. The instantaneous voltage and current increased with increases in the charging voltage, and the voltage and current were approximately 120 kV and 1.0 kA, respectively, at a charging voltage of −70 kV.

B. X-ray output

X-ray output pulse was detected using a combination of a plastic scintillator, a photomultiplier, and the filter (Fig. 6). When the charging voltage was increased, the pulse height increased, but the width seldom varied. The widths were about 70 ns, and the time-integrated x-ray dose measured by a thermoluminescence dosimeter (Kyokko TLD Reader 1500 having MSO-S elements without energy compensation) had an instantaneous value of approximately 70 μGy per pulse at 0.5 m from the x-ray source with a charging voltage of −70 kV.

C. X-ray source

In order to observe the Kα x-ray source, we employed a 100 μm-diameter pinhole camera, an x-ray film (Polaroid XR-7), and the filter (Fig. 7). When the charging voltage was increased, the spot intensity increased, and the intensities corresponded well to the x-ray pulse height. The dimension was almost equal to the target diameter and had a value of about 3.0 mm.

D. X-ray spectra

X-ray spectra were measured using a transmission-type spectrometer[11] with a lithium fluoride curved crystal 0.5 mm in thickness. The x-ray intensities of the spectra were detected by an imaging plate of a computed radiography (CR) system[15] (Konica Regius 150) with a wide dynamic range, and relative x-ray intensity was calculated from Dicom original digital data corresponding to x-ray intensity; the data was scanned by Dicom viewer in the film-less CR system. Subsequently, the relative x-ray intensity as a function of the data was calibrated using a conventional x-ray generator, and we confirmed that the intensity was proportional to the exposure time. Figure 8 shows measured spectra from the molybdenum target with the filter. In fact, we observed clean Kα lines, while bremsstrahlung rays were hardly detected at all. The Kα intensity substantially increased with increases in the charging voltage.

IV. RADIOGRAPHY

The monochromatic flash radiography was performed by the CR system at 0.5 m from the x-ray source with the filter, and the charging voltage was −70 kV.

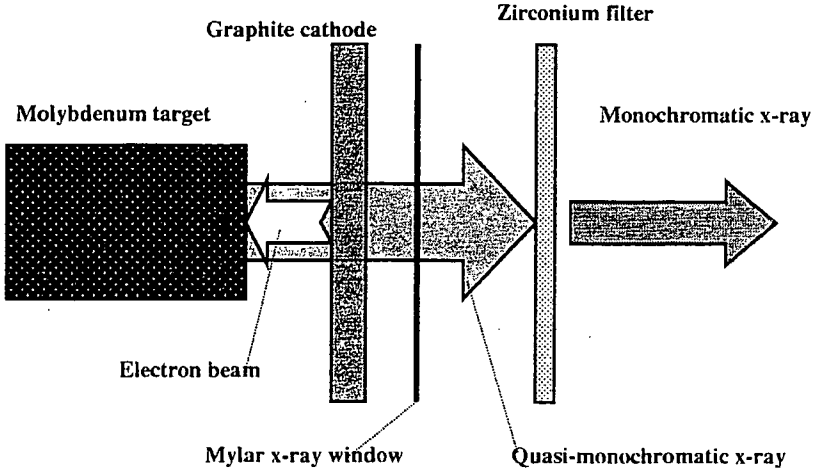

FIG. 4. Irradiation of Kα rays using a monochromatic zirconium filter. Bremsstrahlung rays are not emitted in the opposite direction to that of electron acceleration, and molybdenum Kα rays are left using a zirconium filter.

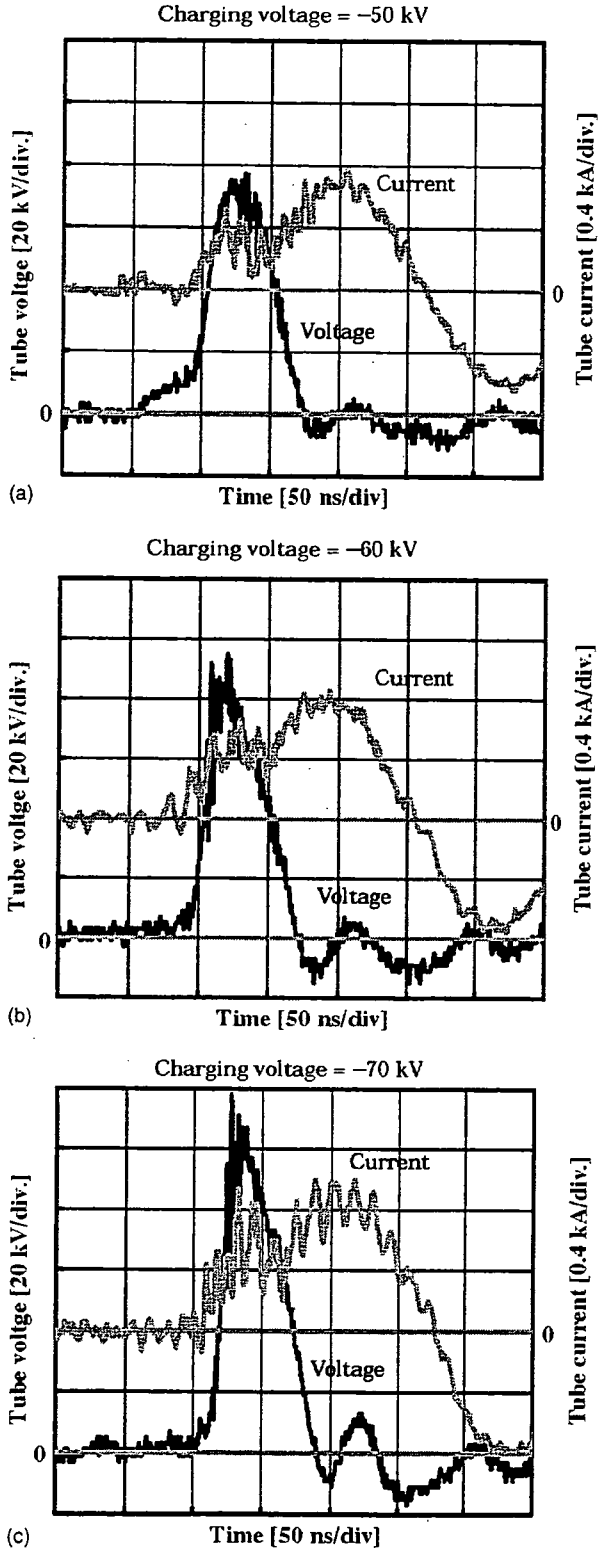

FIG. 5. Variations in the tube voltage and current with a charging voltage of (a) −50 kV, (b) −60 kV, and (c) −70 kV.

First, rough measurements of spatial resolution were made using wires. Figure 9 shows radiograms of tungsten wires coiled around a pipe made of polymethyl methacrylate. Although the image contrast increased with increases in the wire diameter, a 50 μm-diameter wire could be observed.

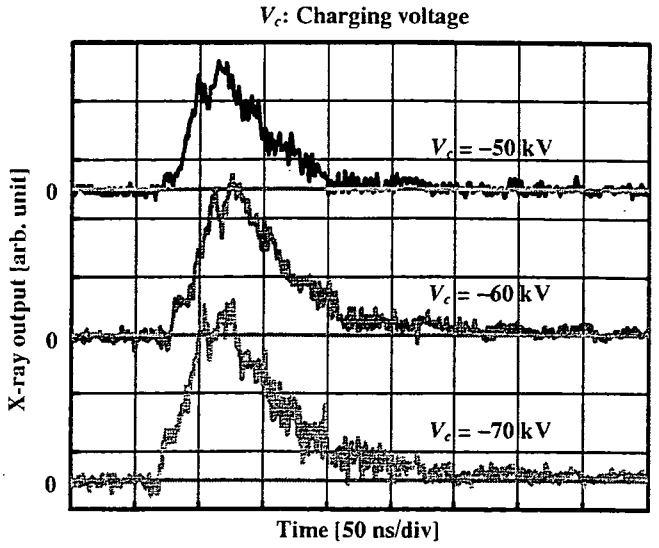

FIG. 6. X-ray outputs detected using a combination of a plastic scintillator, a photomultiplier, and the zirconium filter.

Figure 10 shows a radiogram of a vertebra, and fine structures in the vertebra were observed. Next, the image of water falling into a polypropylene beaker from a glass test tube is shown in Fig. 11. This image was taken with the slight addition of an iodine-based contrast medium. Because the x-ray duration was about 70 ns, the stop-motion image of water could be obtained. Figure 12 shows an angiogram of a rabbit heart; iodine-based microspheres of 15 μm in diameter were used, and fine blood vessels of about 100 μm were visible.

V. DISCUSSION

Concerning the spectrum measurement, we obtained fairly clean molybdenum Kα rays (17.4 keV). Therefore, we are very interested in the measurement the Kα rays from nickel (7.47 keV), copper (8.04 keV), silver (22.1 keV), cerium (34.6 keV), and tungsten (58.9 keV) targets; the target element should be selected corresponding to the radiographic objectives. In a medical application, K-series characteristic x rays of cerium are absorbed effectively by an iodine-based contrast medium with a K-edge of 33.2 keV, and high contrast microangiography can be performed.

In this research, the generator produced instantaneous number of Kα photons was approximately 3×10^7

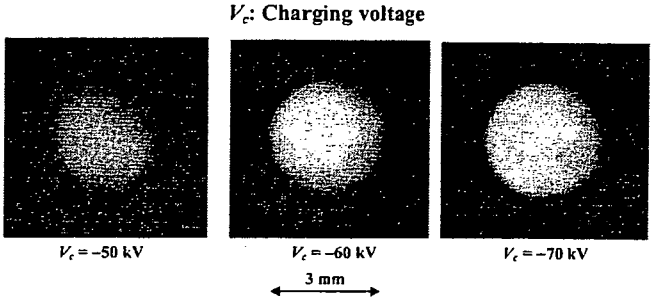

FIG. 7. Images of the x-ray source of Kα lines obtained using a pinhole camera with changes in the charging voltage.

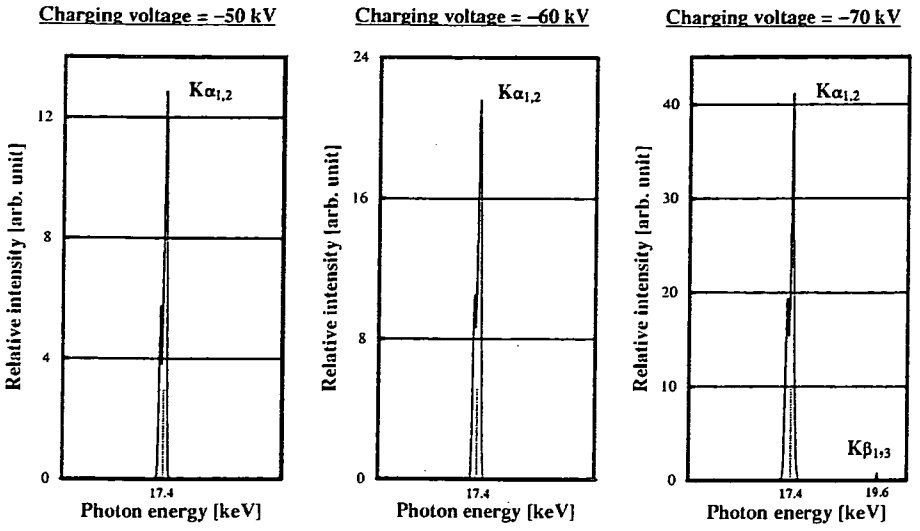

FIG. 8. X-ray spectra from the molybdenum target with the filter. The spectra were measured using a transmission type spectrometer with a lithium fluoride curved crystal.

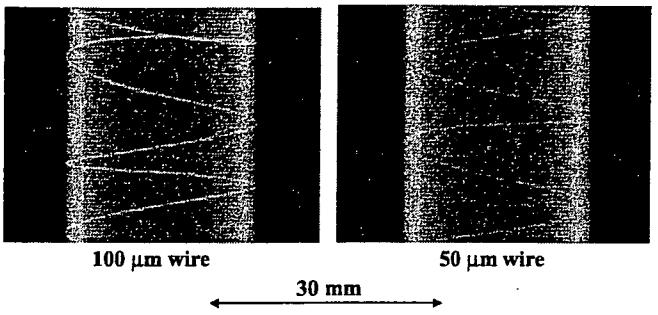

FIG. 9. Radiograms of tungsten wires of 50 and 100 μm in diameter coiled around a pipe made of polymethyl methacrylate. A 50 μm-diameter wire could be observed.

photons/cm^2 per pulse at 0.5 m from the source. Because the molybdenum plasma generator produced approximately 5 $\times 10^8$ photons/cm^2 per pulse at 1.0 m from the source, the x-ray intensity of Kα lines had a lower value as compared with the plasma x-ray generator[11] described above, which utilizes a large capacity condenser of approximately 200 nF. However, the intensity can be increased by increasing the electrostatic energy in condensers in the surge generator, and quasi-monochromatic x rays of both Kα and Kβ (19.6 keV) lines are produced without using the zirconium filter with a K-edge of 17.9 keV.

Using this flash x-ray generator, the photon energy of characteristic x rays can be selected, and we plan to design a high-speed photon-counting radiography system in order to decrease noise from radiograms. In addition, steady-state

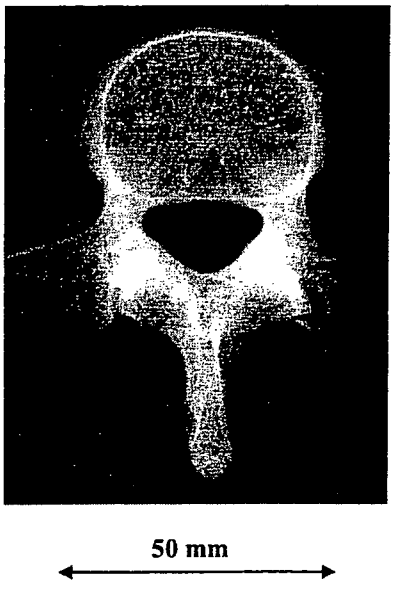

FIG. 10. Radiogram of a vertebra. Fine structure of the vertebra were visible.

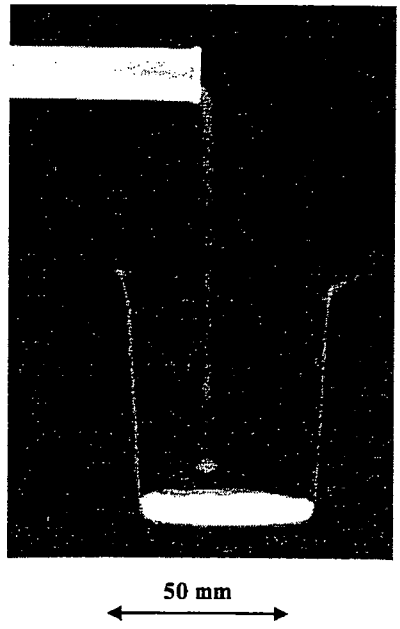

FIG. 11. Radiogram of water falling into a polypropylene beaker from a glass test tube. The stop-motion image of water was obtained by monochromatic flash radiography.

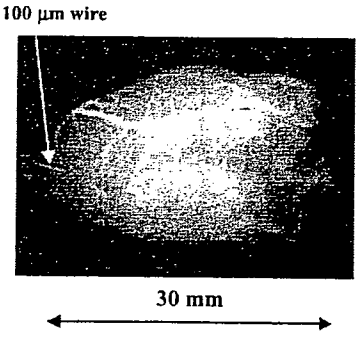

FIG. 12. Angiograms of a rabbit heart. Fine blood vessels of approximately 100 μm were visible.

monochromatic x rays for fluoroscopy can be produced by a similar tube using a constant high-voltage power supply. In conjunction with the fine focusing, these low-cost monochromatic x-ray generators will be employed to perform K-edge angiography and x-ray phase imaging for edge enhancement.[16]

ACKNOWLEDGMENTS

This work was supported by Grants-in-Aid for Scientific Research (13470154, 13877114, and 16591222) and Advanced Medical Scientific Research from MECSST, Grants from Keiryo Research Foundation, The Promotion and Mutual Aid Corporation for the Private School of Japan, JST (Test of Fostering Potential), NEDO, and MHLW (HLSRG, RAMT-nano-001, RHGTEFB-genome-005, and RGCD13C-1).

[a]Electronic mail: dresato@iwate-med.ac.jp

[1]J. J. Rocca, V. Shlyaptsev, F. G. Tomasel, O. D. Cortazar, D. Hartshorn, and J. L. A. Chilla, "Demonstration of a discharge pumped table-top soft x-ray laser," Phys. Rev. Lett. **73**, 2192–2195 (1994).

[2]J. J. Rocca, D. P. Clark, J. L. A. Chilla, and V. N. Shlyaptsev, "Energy extraction and achievement of the saturation linit in a discharge-pumped table-top soft x-ray amplifier," Phys. Rev. Lett. **77**, 1476–1479 (1996).

[3]C. D. Macchietto, B. R. Benware, and J. J. Rocca, "Generation of millijoule-level soft-x-ray laser pulses at a 4-Hz repetition rate in a highly saturated tabletop capillary discharge amplifier," Opt. Lett. **24**, 1115–1117 (1999).

[4]E. Sato, H. Isobe, and F. Hoshino, "High intensity flash x-ray apparatus for biomedical radiography," Rev. Sci. Instrum. **57**, 1399–1408 (1986).

[5]A. Shikoda, E. Sato, M. Sagae, T. Oizumi, Y. Tamakawa, and T. Yanagisawa, "Repetitive flash x-ray generator having a high-durability diode driven by a two-cable-type line pulser," Rev. Sci. Instrum. **65**, 850–856 (1994).

[6]E. Sato, K. Takahashi, M. Sagae, S. Kimura, T. Oizumi, Y. Hayasi, Y. Tamakawa, and T. Yanagisawa, "Sub-kilohertz flash x-ray generator utilizing a glass-enclosed cold-cathode triode," Med. Biol. Eng. Comput. **32**, 289–294 (1994).

[7]K. Takahashi, E. Sato, M. Sagae, T. Oizumi, Y. Tamakawa, and T. Yanagisawa, "Fundamental study on a long-duration flash x-ray generator with a surface-discharge triode," Jpn. J. Appl. Phys., Part 1 **33**, 4146–4151 (1994).

[8]E. Sato, K. Takahashi, M. Sagae, S. Kimura, T. Oizumi, Y. Hayasi, Y. Tamakawa, and T. Yanagisawa, "Sub-kilohertz flash x-ray generator utilizing a glass-enclosed cold-cathode triode," Med. Biol. Eng. Comput. **32**, 289–294 (1994).

[9]E. Sato, R. Germer, Y. Hayasi, E. Tanaka, H. Mori, T. Kawai, T. Usuki, K. Sato, H. Obara, M. Zuguchi, T. Ichimaru, H. Ojima, K. Takayama, and H. Ido, "Plasma flash x-ray generator (PFXG-02)," Proc. SPIE **4948**, 604–609 (2002).

[10]E. Sato, Y. Hayasi, R. Germer, E. Tanaka, H. Mori, T. Kwai, T. Ichimaru, K. Takayama, and Hideaki Ido, "Quasi-monochromatic flash x-ray generator utilizing weakly ionized linear copper plasma," Rev. Sci. Instrum. **74**, 5236–5240 (2003).

[11]E. Sato, Y. Hayasi, R. Germer, E. Tanaka, H. Mori, T. Kawai, H. Obara, T. Ichimaru, K. Takayama, and H. Ido, "Irradiation of intense characteristic x-rays from weakly ionized linear molybdenum plasma," Jpn. J. Med. Phys. **23**, 123–131 (2003).

[12]E. Sato, Y. Hayasi, R. Germer, E. Tanaka, H. Mori, T. Kawai, H. Obara, T. Ichimaru, K. Takayama, and H. Ido, "Intense characteristic x-ray irradiation from weakly ionized linear plasma and applications," Jpn. J. Med. Imag. Inform. Sci. **20**, 148–155 (2003).

[13]A. Mattsson, "Some characteristics of a 600 kV flash x-ray tube," Phys. Scr. **5**, 99–102 (1972).

[14]R. Germer, "X-ray flash techniques," J. Phys. E **12**, 336–350 (1979).

[15]E. Sato, K. Sato, and Y. Tamakawa, "Film-less computed radiography system for high-speed imaging," Ann. Rep. Iwate Med. Univ. Sch. Lib. Arts Sci. **35**, 13–23 (2000).

[16]A. Ishisaka, H. Ohara, and C. Honda, "A new method of analyzing edge effect in phase contrast imaging with incoherent x-rays," Opt. Rev. **7**, 566–572 (2000).

Available online at www.sciencedirect.com
SCIENCE DIRECT
Neuroscience Letters 388 (2005) 61–64
Neuroscience Letters
www.elsevier.com/locate/neulet

Contribution of catechol *O*-methyltransferase to the removal of accumulated interstitial catecholamines evoked by myocardial ischemia

Yosuke Kuroko [a], Takafumi Fujii [a], Toji Yamazaki [b,*], Tsuyoshi Akiyama [b], Kozo Ishino [a], Shunji Sano [a], Hidezo Mori [b]

[a] *Department of Cardiovascular Surgery, Okayama University Graduate School of Medicine and Dentistry, Okayama 700-8558 Japan*
[b] *Department of Cardiac Physiology, National Cardiovascular Center Research Institute, 5-7-1 Fujishiro-dai, Suitâ, Osaka 565-8565 Japan*

Received 7 May 2005; received in revised form 15 June 2005; accepted 16 June 2005

Abstract

Catechol *O*-methyltransferase (COMT) plays an important role for clearance of high catecholamine levels. Although myocardial ischemia evokes similar excessive catecholamine accumulation, it is uncertain whether COMT activity is involved in the removal of accumulated catecholamines evoked by myocardial ischemia. We examined how COMT activity affects myocardial catecholamine levels during myocardial ischemia and reperfusion. We implanted a dialysis probe into the left ventricular myocardial free wall and measured dialysate catecholamines levels in anesthetized rabbits. Dialysate catecholamine levels served as an index of myocardial interstitial catecholamine levels. We introduced myocardial ischemia by 60 min occlusion of the main coronary artery. The ischemia-induced dialysate catecholamines levels were compared with and without the pretreatment with entacapone (COMT inhibitor, 10 mg/kg, i.p.). Acute myocardial ischemia progressively increased dialysate catecholamine levels. Acute myocardial ischemia increased dialysate norepinephrine (NE) levels (20,453 ± 7186 pg/ml), epinephrine (EPI) levels (1724 ± 706 pg/ml), and dopamine (DA) levels (1807 ± 800 pg/ml) at the last 15 min of coronary occlusion. Inhibition of COMT activity by entacapone augmented the ischemia-induced NE levels (54,306 ± 6618 pg/ml), EPI levels (2681 ± 567 pg/ml), and DA (3551 ± 710 pg/ml) levels at the last 15 min of coronary occlusion. Myocardial ischemia evoked NE, EPI, and DA accumulation in the myocardial interstitial space. The inhibition of COMT activity augmented these increments in NE, EPI, and DA. These data suggest that cardiac COMT activity influences on the removal of accumulated catecholamine during myocardial ischemia.

Keywords: Catecholamine; Microdialysis; Myocardial infarction; Heart; Catechol *O*-methyltransferase

Myocardial ischemia evokes an excessive norepinephrine (NE) accumulation in the myocardial interstitial space [2,15]. Interstitial NE is largely removed by NE transport into the sympathetic nerve endings and metabolized to dihydroxyphenylglycol (DHPG) via monoamine oxidase (MAO) [6,22]. The remainder spills over into the coronary sinus [6]. However, during myocardial ischemia, two important NE removing systems are impaired. Myocardial ischemia reduces coronary flow, which abolishes NE spillover. Furthermore, membrane NE transport is dependent on the Na^+ gradient between the extracellular and intracellular spaces. During ischemia, NE uptake is blocked and outward NE transport through the uptake$_1$ carrier is induced by the reduced Na^+ gradient [17]. Thus, production of DHPG via MAO is inhibited by myocardial ischemia [1]. Up to now, little has been known about the role of catechol *O*-methyltransferase (COMT) in the removal of interstitial NE. Catechol *O*-methyltransferase has been believed to be operative only at high concentrations of NE via NE infusion [12]. An excessive NE accumulation in the myocardial ischemia was similar to NE levels in

* Corresponding author. Tel.: +81 6 6833 5012x2379; fax: +81 6 6872 8092.
E-mail address: yamazaki@ri.ncvc.go.jp (T. Yamazaki).

0304-3940/$ – see front matter © 2005 Elsevier Ireland Ltd. All rights reserved.
doi:10.1016/j.neulet.2005.06.031

intravenous NE infusion. Therefore, this NE removal system may be the sole mechanism that decreases myocardial interstitial NE.

Recent study has demonstrated that myocardial ischemia is associated with a pronounced increase in the concentration of endogenous NE, epinephrine (EPI), dopamine (DA) in the myocardial interstitial space [14]. These accumulated catecholamines may be a candidate of substrate of COMT. However, in most experiments on COMT activity, isoprenaline was used as the substrate of COMT [11,19] since it is not a substrate for neuronal uptake and MAO activity. Furthermore, data on isolated perfused lungs suggest that the affinity of COMT activity for *O*-methylation differed among the three amines [3]. It is uncertain whether COMT activity is involved in the removal of accumulated interstitial catecholamines evoked by myocardial ischemia.

In the present study, the possibility that the concentration of these three catecholamines in the myocardial interstitial space was affected by COMT activity was examined in anesthetized myocardial ischemic rabbits. With the use of dialysis technique, a dialysis probe was implanted into the left ventricle free wall perfused by the main branch of left circumflex coronary artery (LCX) to measure myocardial interstitial catecholamines levels in the ischemic region and dialysate catecholamines levels were compared in the absence and presence of COMT inhibitor.

Animal care proceeded in strict accordance with the *Guide for the Care and Use of Laboratory Animals* published by the US National Institutes of Health (NIH Publication No. 85-23, revised 1996). Adult male Japanese white rabbits (2.5–3.2 kg) were anesthetized with pentobarbital sodium (30–35 mg/kg i.v.). The level of anesthesia was maintained with a continuous intravenous infusion of pentobarbital sodium (1–2 mg/kg/h). The rabbits were intubated and ventilated with room air mixed with oxygen. Heart rate, arterial pressure, and electrocardiogram were simultaneously monitored with a data recorder. The fifth or sixth rib on the left side was partially removed to expose the heart. A 4–0 silk suture was passed around the main branch of LCX, to act as the occluder for later coronary occlusion. With a fine guiding needle, a dialysis probe was implanted in the region perfused by LCX of the left ventricular wall. Judging from changes in the color of the ventricular wall during a brief coronary occlusion, the dialysis probe was located in the midst of the ischemic region. Heparin sodium (100 IU/Kg) was administered intravenously to prevent blood coagulation.

The dialysate NE, EPI, and DA levels were measured as an index of myocardial interstitial NE, EPI, and DA levels, respectively. A dialysis fiber (8 mm length, 0.31 mm o.d., and 0.20 mm i.d.; PAN-1200 50,000 molecular weight cutoff, Asahi Chemical Japan) was glued at both ends of a polyethylene tube. The dialysis probe was perfused with Ringer's solution at a perfusion speed of 2 μl/min. Dialysate NE level was measured by the first HPLC after removing interfering compounds by the alumina procedure [23]. Dialysate EPI and DA levels were measured by direct injection into the second HPLC [18].

After control sampling, we occluded the main branch of LCX for 60 min and then released the occluder. The 15-min dialysate samples were collected before, during and after 60 min LCX occlusion. In vehicle group, we administered saline intraperitoneally as vehicle 120 min before control sampling. After control sampling, we observed the time course of dialysate NE, EPI, and DA levels from the ischemic region during 60 min of coronary occlusion and 15 min of reperfusion. To elucidate the role of COMT activity in the ischemia-induced changes in myocardial interstitial NE EPI, and DA levels, we compared dialysate NE, EPI, and DA levels in the ischemic region with those levels after injection of COMT inhibitor. We administered intraperitoneally the COMT inhibitor entacapone (10 mg/kg; Orion-Pharma, Espoo, Finland) 120 min before control sampling. Entacapone was dissolved in phosphate buffered saline, the pH of the solution was adjusted to 7.4, and the dose of entacapone was determined based on the dose used in the earlier preliminary experiments [7,8].

Changes in the dialysate NE levels in the vehicle and the pretreatment with entacapone are shown in Fig. 1. In the vehicle group, dialysate NE level averaged from six rabbits was 52 ± 12 pg/ml in the control. During 60 min coronary occlusion, dialysate NE levels markedly increased. The dialysate NE levels reached up to 400 times the control levels during the last 15 min of 60 min coronary occlusion. After release of the occluder, dialysate NE levels rapidly decreased to 3473 ± 735 pg/ml, although their levels were higher than those in the control. In the presence of entacapone, dialysate NE levels also markedly increased during 60 min coronary occlusion. The dialysate NE levels reached up to 1000 times the control levels during the last 15 min of 60 min coronary occlusion. These increases in dialysate NE levels at 15–60 min of coronary occlusion were significantly enhanced by entacapone whereas entacapone did not change dialysate NE levels in the control (51 ± 16 pg/ml) or at 0–15 min of

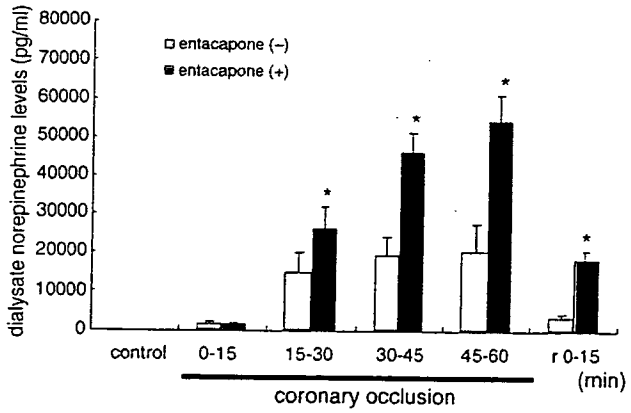

Fig. 1. Dialysate norepinephrine levels before, during and after 60 min-coronary occlusion. Values are mean ± S.E. ($n = 6$). $^*P < 0.05$ vs. concurrent value of vehicle group.

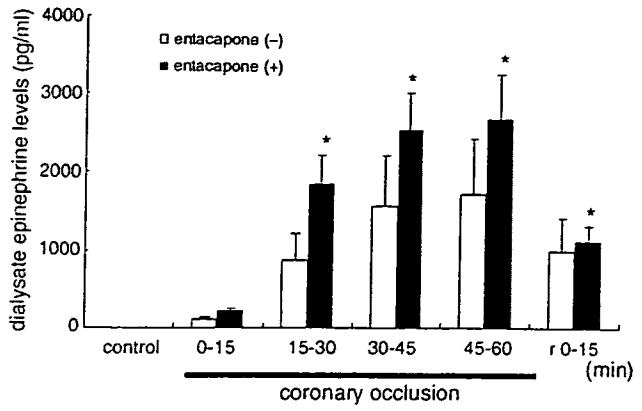

Fig. 2. Dialysate epinephrine levels before, during and after 60 min-coronary occlusion. Values are mean ± S.E. ($n = 6$). $^*P < 0.05$ vs. concurrent value of vehicle group.

coronary occlusion. Dialysate NE levels decreased by reperfusion, but remained higher than those in vehicle group. Thus, COMT activity for NE removal was operative in ischemic and reperfusion periods. Entacapone augmented peak NE levels to 160% of vehicle group.

Dialysate EPI levels were below the detectable level in the control. After coronary occlusion, dialysate EPI levels gradually increased and reached 1724 ± 706 pg/ml at 45–60 min of occlusion (Fig. 2). Peak EPI levels during the ischemia were one-twentieth of NE levels during the ischemic period. In the presence of entacapone, dialysate EPI levels were below the detectable level in the control. Dialysate EPI levels gradually increased during coronary occlusion and reached 2681 ± 567 pg/ml at 45–60 min of occlusion. In the presence of entacapone, dialysate EPI levels at 15–60 min of the ischemia were higher than those in the vehicle group. Entacapone augmented peak EPI levels by 50% of vehicle group.

Dialysate DA levels were below the detectable level in the control and at 0–15 min of ischemia. After 15 min of occlusion, dialysate DA levels gradually increased and reached 1807 ± 800 pg/ml at 45–60 min of occlusion (Fig. 3). Peak DA levels during the ischemia were one-twentieth of NE

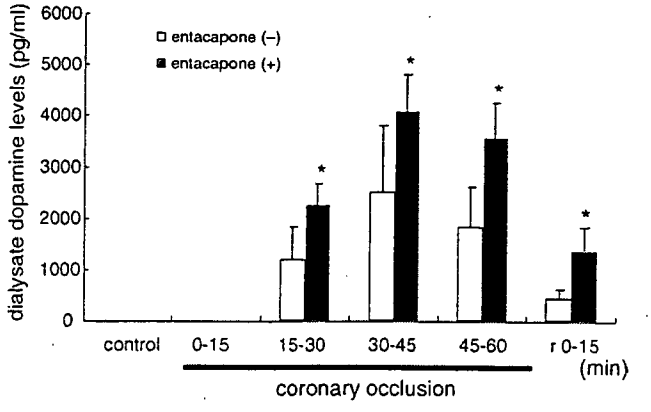

Fig. 3. Dialysate dopamine levels before, during and after 60 min-coronary occlusion. Values are mean ± S.E. ($n = 6$). $^*P < 0.05$ vs. concurrent value of vehicle group.

levels during the ischemia. In the presence of entacapone, dialysate DA levels were below the detectable level in the control and at 0–15 min of the occlusion. Dialysate DA levels gradually increased during 15–60 min of the ischemia and reached 3351 ± 710 pg/ml at 45–60 min of occlusion. In the presence of entacapone, dialysate DA levels at 15–60 min of the ischemia were higher than those in the vehicle group. Entacapone augmented peak DA levels by 100% of vehicle group.

Myocardial ischemia induced a progressive increase of interstitial catecholamines. The rank order of the amount of catecholamine release was NE much greater than EPI or DA, with this rank order remaining unchanged before, during and after myocardial ischemia. These findings are in line with those reported by Lameris et al. [14] studied the time course of myocardial interstitial catecholamine levels during myocardial ischemia. The measurement of overall content in the left ventricle free wall was performed in dogs [13] and the in vitro ratio of EPI/NE or DA/NE was similar to our result. Therefore, the rank order may reflect the ratio of overall catecholamine content in the left ventricle free wall.

In the resting state and early period (0–15 min) of ischemia, COMT does not appear to contribute to the removal of myocardial interstitial catecholamine levels. In the mid-late period of ischemia, COMT contributes to the inactivation of high myocardial interstitial catecholamine levels evoked by ischemia. The rank order of the amount of neurotransmitter release was NE much greater than EPI or DA. From percentage increase of catecholamine by entacapone, the rank order of COMT activity for removal of catecholamines was considered to be NE greater than DA greater than EPI. On the other hand, when catecholamines were infused in the isolated rat heart, the metabolism of the catecholamines by COMT differs: DA = NE less than EPI [9]. These data suggest that contribution of COMT to removal of accumulated catecholamines depends on the types of amines and the amount of accumulated catecholamine. In the absence of catecholamine spill over and MAO activity, COMT might constitutes one of major pathways of catecholamine metabolism in ischemic heart. Alternatively all three catecholamines are taken up and then metabolized by COMT at the extraneuronal tissues [4,10]. Uptake and *O*-methylation may handle three catecholamines in a different manner.

Up to now, little has been known about the role of cardiac COMT activity in the removal of accumulated interstitial catecholamine. In the isolated perfused rat, Carlsson et al. [5], demonstrated that marked NE release was paralleled by an increasing extraneuronal inactivation of released NE. Accumulated catecholamine in myocardial interstitial space is involved in the pathophysiology of ischemic heart disease [16,21]. Therefore, these data suggest that inhibition of COMT activity deteriorates myocardial ischemic injury via enhanced catecholamine accumulation. In contrast to this hypothesis, Valenza et al. [20], demonstrated that the inhibition of COMT (by nitecapone) improved the mechanical function of the heart during ischemia-reperfusion injury. In

the present study, we did not measure myocardial contractile function or biochemical markers. Future work should concentrate on these aspects of COMT action during myocardial ischemia.

Acknowledgement

This work was supported by Grands-in-Aid for scientific research (15590787) from the Ministry of Education, Culture, Sports, Science and Technology. The authors thank Orion-Pharma (Espoo, Finland) for the supply of entacapone.

References

[1] T. Akiyama, T. Yamazaki, Myocardial interstitial norepinephrine and dihydroxyphenylglycol levels during ischemia and reperfusion, Cardiovasc. Res. 49 (2001) 78–85.
[2] T. Akiyama, T. Yamazaki, I. Ninomiya, Differential regional responses of myocardial interstitial noradrenaline levels to coronary occlusion, Cardiovasc. Res. 27 (1993) 817–822.
[3] L.J. Bryan-Lluka, S.R. O'Donnell, Dopamine and adrenaline, but not isoprenaline, are substrates for uptake and metabolism in isolated perfused lungs of rats, Naunyn Schmiedebergs Arch. Pharmacol. 346 (1992) 20–26.
[4] C. Burgdorf, A. Dendorfer, T. Kurz, E. Schömig, I. Stolting, F. Schutte, G. Richardt, Role of neuronal KATP channels and extraneuronal monoamine transported on norepinephrine overflow in a model of myocardial low flow ischemia, J. Pharmacol. Exp. Ther. 309 (2004) 42–48.
[5] L. Carlsson, T. Abrahamsson, O. Almgren, Release of noradrenaline in myocardial ischemia-importance of local inactivation by neuronal and extraneuronal mechanisms, J. Cardiovasc Pharmacol. 8 (1986) 545–553.
[6] G. Eisenhofer, J.J. Smolich, H.S. Cox, M.D. Esler, Neuronal reuptake of norepinephrine and production of dihydroxyphenylglycol by cardiac sympathetic nerve in the anesthetized dog, Circulation 84 (1991) 1354–1363.
[7] T. Fujii, T. Yamazaki, T. Akiyama, S. Sano, H. Mori, In vivo assessment of catechol *O*-methyltransferase activity in rabbit skeletal muscle, Auton. Neurosci. 111 (2004) 140–143.
[8] T. Fujii, T. Yamazaki, T. Akiyama, S. Sano, H. Mori, Extraneuronal enzymatic degradation of myocardial norepinephrine in the ischemic region, Cardiovasc. Res. 64 (2004) 125–131.
[9] M. Grohmann, The activity of the neuronal and extraneuronal catecholamine metabolizing enzymes of the perfused rat heart, Naunyn Schmiedebergs Arch. Pharmacol. 336 (1987) 139–147.
[10] M. Grohmann, U. Trendelenburg, The handling of five catecholamines by the extraneuronal *O*-methylating system of the rat heart, Naunyn Schmiedebergs Arch. Pharmacol. 329 (1985) 264–270.
[11] M. Inoue, K. Hifumi, K. Kurahashi, M. Fujiwara, Impairment of the extraneuronal *O*-methylating system of isoproterenol by stop-flow ischemia in the perfused rat heart, J. Pharmacol. Exp. Ther. 242 (1987) 1086–1089.
[12] L.L. Iversen, P.J. The uptake of catechol amines at high perfusion concentrations in the rat isolated heart: a novel catechol amine uptake process, Br. J. Pharmacol. 25 (1965) 18–33.
[13] W.R. Kaufman, B.I. Jugdutt, Left ventricular catecholamines during acute myocardial infarction in the dog, Can. J. Physiol. Pharmacol. 65 (1987) 172–178.
[14] T.W. Lameris, S. deZeeuw, G. Alberts, F. Boomsma, D.J. Duncker, P.D. Verdouw, A.J. Man in't Veld, A.H. van den Meiracker, Time course and mechanism of myocardial catecholamine release during transient ischemia in vivo, Circulation 101 (2000) 2645–2650.
[15] P. Mertes, K. El-Abbassi, Y. Jabpin, C. Michel, B. Beck, G. Pinelli, J. Carteaux, J. Villemot, C. Burlet, Consequences of coronary occlusion on changes in regional interstitial myocardial neuropeptide Y and norepinephrine concentrations, J. Mol. Cell. Cardiol. 28 (1996) 1995–2004.
[16] W.J. Penny, The deleterious effects of myocardial catecholamines on cellular electrophysiology and arrhythmias during ishaemia and reperfusion, Eur. Heart J. 5 (1984) 960–973.
[17] A. Schömig, T. Kurz, G. Richardt, E. Schömig, Neuronal sodium homeostatis and axoplasmic amine concentration determine calcium-independent noradrenaline release in normoxic and ischemic rat heart, Circ. Res. 63 (1988) 214–226.
[18] N. Tokunaga, T. Yamazaki, T. Akiyama, H. Mori, Detection of 3-methoxy-4-hydroxyphenylglycol in rabbit skeletal muscle microdialysate, J. Cnromatogr. B. 798 (2003) 163–166.
[19] U. Trendelenburg, H. Fleig, L.J. Bryan, H. Bönisch, The extraneuronal compartments for the distribution of isoprenaline in the rat heart, Naunyn Schmiedebergs Arch. Pharmacol. 324 (1983) 169–179.
[20] M. Valenza, E. Sarbinova, L. Packer, S. Khwaja, J. Catudioc, Nitecapone protects the Langendorff perfused heart against ischemia-reperfusion injury, Biochem. Mol. Biol. Int. 29 (1993) 443–449.
[21] A.P. Waldenström, A.C. Hjalmarson, L. Thornell, A possible role of noradrenaline in the development of myocardial infarction. An experimental study in the isolated rat heart, Am. Heart. J. 95 (1978) 43–51.
[22] T. Yamazaki, T. Akiyama, H. Kitagawa, T. Kawada, K. Sunagawa, Dialysate dihydroxyphenylglycol as a window for in situ axoplasmic norepinephrine disposition, Neurochem. Int. 38 (2001) 287–292.
[23] T. Yamazaki, T. Akiyama, T. Shindo, Routine high-performance liquid chromatographic determination of the myocardial interstitial norepinephrine, J. Chromatogr. B. 670 (1995) 328–331.

Clean monochromatic x-ray irradiation from weakly ionized linear copper plasma

Eiichi Sato, MEMBER SPIE
Iwate Medical University
Department of Physics
Morioka 020-0015, Japan
E-mail: dresato@iwate-med.ac.jp

Etsuro Tanaka
Tokyo University of Agriculture
Department of Nutritional Science
Faculty of Applied Bioscience
Setagaya-ku 156-8502, Japan

Hidezo Mori
National Cardiovascular Center Research Institute
Department of Cardiac Physiology
Osaka 565-8565, Japan

Toshiaki Kawai, MEMBER SPIE
Hamamatsu Photonics K.K.
Electron Tube Division #2
Iwata-gun 438-0193, Japan

Shigehiro Sato
Iwate Medical University
Department of Microbiology
School of Medicine
Morioka 020-8505, Japan

Kazuyoshi Takayama, MEMBER SPIE
Tohoku University
Shock Wave Research Center
Institute of Fluid Science
Sendai 980-8577, Japan

Abstract. In the plasma flash x-ray generator, a 200-nF condenser is charged up to 50 kV by a power supply, and flash x-rays are produced by the discharging. The x-ray tube is a demountable triode with a trigger electrode, and the turbomolecular pump evacuates air from the tube with a pressure of approximately 1 mPa. Target evaporation leads to the formation of weakly ionized linear plasma, consisting of copper ions and electrons, around the fine target, and intense Kα rays are produced using a 10-μm-thick nickel filter. At a charging voltage of 50 kV, the maximum tube voltage is almost equal to the charging voltage of the main condenser, and the peak current is about 15 kA. When the charging voltage is increased, the linear plasma forms, and the copper Kα intensities substantially increase. The Kα lines are quite clean and intense, and hardly any bremsstrahlung rays are detected at all. The x-ray pulse widths are approximately 700 ns, and the time-integrated x-ray intensity has a value of approximately 20 μC/kg at 1.0 m from the x-ray source with a charging voltage of 50 kV. [DOI: 10.1117/1.1882373]

Subject terms: flash x-ray; weakly ionized linear plasma; copper target; Kα characteristic x-rays; monochromatic x-rays.

Paper 040184 received Mar. 29, 2004; revised manuscript received Sep. 9, 2004; accepted for publication Oct. 25, 2004; published online Mar. 30, 2005. This paper is a revision of a paper presented at SPIE conference on Laser-Generated and Other Laboratory X-Ray and EUV Sources, Optics, and Applications, Aug. 2003, San Diego, California. The paper presented there appears (unrefereed) in SPIE Proceedings Vol. 5196.

1 Introduction

Flash x-rays have been produced by several different methods, and various generators have been developed corresponding to specific radiographic objectives.[1-3] Currently, maximum photon energy has been increased to approximately 1 MeV using multistage Marx pulse generators[1,2] to produce hard x-rays for military studies. In soft x-ray generators,[4-7] high-intensity single generators with large capacity condensers were originally developed. Subsequently, repetitive generators[8-12] have been developed, and the repetition rate has been increased to subkilohertz using a cold-cathode triode.

Recently, soft x-ray lasers have been produced by a gas-discharge capillary,[13-16] and the laser pulse energy substantially increased in proportion to the capillary length. These kinds of fast discharges can generate hot and dense plasma columns with aspect ratios approaching 1000:1. However, it is difficult to increase the laser photon energy to 10 keV or beyond. Because there are no x-ray resonators in the high photon energy region, new methods for increasing coherence will be desired in the future.

0091-3286/2005/$22.00 © 2005 SPIE

We have developed several different plasma flash x-ray generators corresponding to specific radiographic objectives, and a major goal in our research is the development of an intense and clean monochromatic x-ray generator that can impact applications with biomedical radiography. By forming weakly ionized linear plasma,[17-20] because we have succeeded in producing fairly intense and clean quasi-monochromatic x-rays from the plasma axial direction, monochromatic x-rays should be produced using a K-edge filter.

We describe a plasma flash x-ray generator utilizing a new plasma x-ray tube, and used it to perform a preliminary experiment for generating clean monochromatic x-rays by forming a linear copper plasma cloud around a fine target.

2 Generator

2.1 *High-Voltage Circuit*

Figure 1 shows a block diagram of the high-intensity plasma flash x-ray generator. This generator consists of the following essential components: a high-voltage power supply, a high-voltage condenser with a capacity of approximately 200 nF, a turbomolecular pump, a krytron pulse